Article

Role of land-ocean interactions in stepwise Northern Hemisphere Glaciation

Yi Zhong [1] ✉, Ning Tan [2] ✉, Jordan T. Abell [3,4], Chijun Sun [5], Stefanie Kaboth-Bahr[6], Heather L. Ford [7], Timothy D. Herbert [8], Alex Pullen [9], Keiji Horikawa [10], Jimin Yu[11,12], Torben Struve [13], Michael E. Weber [14], Peter D. Clift[15], Juan C. Larrasoaña [16,17], Zhengyao Lu [18], Hu Yang [19], André Bahr [20], Tianyu Chen [21], Jingyu Zhang [1], Cao Wei[1], Wenyue Xia[1], Sheng Yang[1] & Qingsong Liu[1,22] ✉

The investigation of triggers causing the onset and intensification of Northern Hemisphere Glaciation (NHG) during the late Pliocene is essential for understanding the global climate system, with important implications for projecting future climate changes. Despite their critical roles in the global climate system, influences of land-ocean interactions on high-latitude ice sheets remain largely unexplored. Here, we present a high-resolution Asian dust record from Ocean Drilling Program Site 1208 in the North Pacific, which lies along the main route of the westerlies. Our data indicate that atmosphere-land-ocean interactions affected aeolian dust emissions through modulating moisture and vegetation in dust source regions, highlighting a critical role of terrestrial systems in initiating the NHG as early as 3.6 Myr ago. Combined with additional multi-proxy and model results, we further show that westerly wind strength was enhanced, mainly at low-to-middle tropospheric levels, during major glacial events at about 3.3 and 2.7 Myr ago. We suggest that coupled responses of Earth's surface dynamics and atmospheric circulation in the Plio-Pleistocene likely involved feedbacks related to changes in paleogeography, ocean circulation, and global climate.

The onset and intensification of Northern Hemisphere Glaciation (NHG) occurred from the mid-Pliocene to the early Pleistocene (ca. 3.6–2.5 Myr ago), and represented a major climatic transition within the broader, gradual Neogene cooling[1,2]. Proposed mechanisms responsible for the onset and intensification of NHG (hereafter referred to as "oNHG" and "iNHG", respectively) have mainly focused on factors such as decreasing atmospheric CO_2[3,4], polar ocean stratification[5], and tectonic changes affecting the configuration of major oceanic gateways including the Bering Strait, the Indonesian seaway, and Central American seaway[6]. Although teleconnections between the terrestrial and marine components of the Earth System can critically affect global climate[7], their potential impacts during the oNHG at ~3.6 million years ago and iNHG at ~2.7 million years ago have received less attention[2].

To elucidate the role of land-ocean teleconnections, we investigate marine dust records that contain clues about environmental conditions of the dust source regions as well as the intensity/position of transporting agents (such as wind, water, and ice)[8–11]. Pelagic North Pacific Ocean sediments provide a unique archive for reconstructing windblown dust delivered from the arid interior of Central and East Asia and the associated Northern Hemisphere westerlies (Fig. 1). Previous studies in the North Pacific have focused either on the driving mechanisms for enhanced aeolian dust production[8,12] or the characteristics of wind systems transporting dust[12,13]. These studies show that, in addition to the moisture budget in dust source regions of Central and East Asia, the latitudinal position and strength of prevailing westerly winds might also have influenced the temporal variability
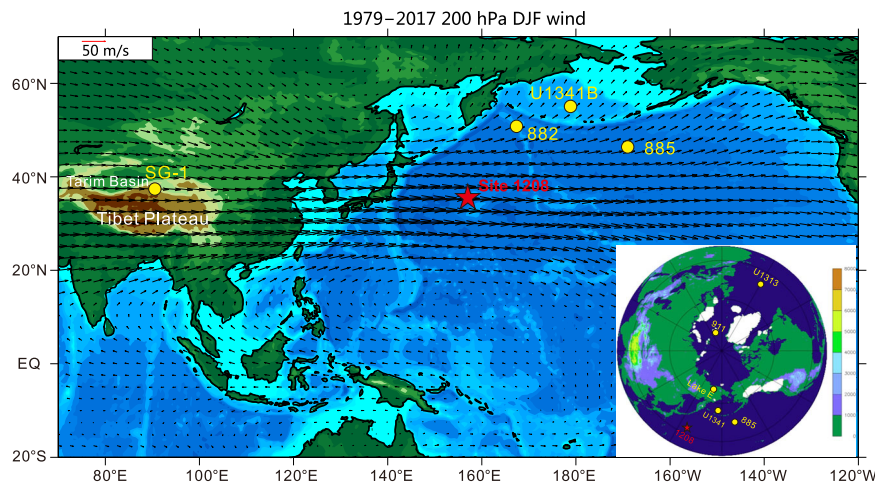
Fig. 1 | Regional wind and topography. Modern (1979-2017) 200hPa winds over the Pacific Ocean and East Asia in boreal winter (December-January-February), using NCEP Reanalysis 2 data. The inset shows the topography reconstructed by the PlioMIP phase 1[71] and the simulated Northern Hemisphere ice sheet coverage during MIS M2[3]. Red star denotes studied Ocean Drilling Program (ODP) Site 1208 and yellow circles represent literature marine and paleolake sites with dust proxy records discussed within the text.

of aeolian dust fluxes to the North Pacific Ocean[13]. Furthermore, several high-resolution studies previously revealed that dust deposition in the North Pacific increased between ca. 2.74 and 2.72 Myr ago, coeval with the establishment of large-scale perennial Northern Hemisphere Ice Sheets (NHIS)[13,14] (Fig. 2a). As previously noted[13], the timing for mid-latitude North Pacific dust flux enhancement is concomitant with the first substantial rise in dust fluxes into the North Atlantic[15] (Fig. 2i) and the Southern Ocean[16] (Fig. 2j), indicating a tight interhemispheric connection between enhanced global dust inputs and global cooling during the late Pliocene. While previous studies have suggested that variations in the position and intensity of the westerlies were governed by similar mechanisms for times before the iNHG[13,14], the connection between pre-iNHG dust fluxes to the North Pacific Ocean and the underlying mechanisms triggering the oNHG remain uncertain. This uncertainty persists because of the scarcity of continuous, well-dated North Pacific dust records with sub-orbital resolution for the period before ca. 3 Myr ago[13,14].

Here we fill this critical gap by providing high-resolution rock magnetic and geochemical records for Ocean Drilling Program (ODP) Site 1208 (Fig. 1). ODP Site 1208 is well positioned to constrain Asian dust inputs and sedimentation in the North Pacific during the middle and late Pliocene (4.0−2.5 Myr ago)[17]. Combined with available stable isotope stratigraphy (ca. 3.7−1.7 Myr ago)[18] and extra-terrestrial ³He-derived sediment fluxes (ca. 4.5−2.5 Myr ago)[13], our data indicate increased aeolian dust input to the North Pacific during periods when NHIS formed and expanded throughout the Pliocene. We propose that the vegetation turnover in Central Asia and dust inputs to the Pacific in the mid-Pliocene could promote a link between ice-sheet formation, land-surface albedo, and ocean-atmosphere coupling. We also present climate simulations to support the notion that the waxing and waning of NHIS representing cold and warm intervals, respectively, during the middle-Pliocene and early Pleistocene can substantially alter the characteristics of the westerlies, and thus dust transport into the North Pacific Ocean.

Results and discussion

Plio-Pleistocene dust evolution in the North Pacific Ocean

Elemental (La-Th-Sc) and radiogenic Pb isotope data, along with previously published Nd and Sr isotope data[19] show that detrital fractions of sediments at ODP Site 1208 are sourced from Asian dust and circum-Pacific volcanic detritus[20], with the Taklimakan Desert as the dominant source of dust[19] (Supplementary Fig. 1a−c). Dust from Central and East Asia contains abundant haematite (Hm) and goethite (Gt)[21], and acts as the primary control on the overall Hm and Gt signals in depositional settings where aeolian dust constitutes the majority of the terrestrial input[22]. We thus use the flux of Hm and Gt (Rel_{Hm+Gt} flux) at ODP Site 1208 as a proxy for Asian dust inputs to the North Pacific (see Material and Methods), with higher fluxes reflecting enhanced atmospheric dust inputs into the ocean.

Our Rel_{Hm+Gt} flux record reflects the timing and nature of North Pacific dust flux variability during the middle to late Pliocene, with a sufficient temporal resolution to resolve sub-orbital changes over 4.0−2.5 Myr ago (Fig. 2c, d). The baseline of Rel_{Hm+Gt} flux minima remains remarkably invariant from 4.0−2.5 Myr ago, with increased fluxes associated mostly with cold (glacial) periods (Fig. 2a). Of note, our data reveal noteworthy variations across three major glacial periods. Firstly, an initial enhancement of aeolian inputs observed at both western (ODP Site 1208) and central North Pacific (ODP Site 885) at ca. 3.6 Myr ago (Fig. 2b), accompanied by a shift in the vegetation of Central Asia (Fig. 3d). These coeval changes corresponded to an ice-rafted detritus (IRD) peak in the Arctic Ocean at the oNHG[23] (Fig. 3c). Considering the previously proposed connection between late Pliocene ice sheet extent and dust fluxes to the ocean[13], our data are consistent with the notion that initial variations in NHIS volume can be traced back to Marine Isotope Stage (MIS) Gi2 (Fig. 2a), when the NHIS was relatively small in spatial extent and short in duration[24,25]. Secondly, dust flux greatly increased from ca. 3.31 to 3.28 Myr ago (glacial MIS M2), which was a globally pronounced cooling event that disturbed the climate of the mid-Piacenzian Warm Period (mPWP, ca. 3.3−3.0 Myr ago)[26,27]. The interval following the mPWP was characterized by larger fluctuations in dust fluxes, including pronounced dust peaks during pre-iNHG glacial intervals (MIS KM2 and G20). Thirdly, the iNHG is marked by a prominent dust peak at 2.73 Myr ago (Fig. 2c and d), after which dust inputs during glacial maxima seem to have varied proportionally to the global ice volume, as reflected by benthic oxygen isotopes[28] (Fig. 2a). Pleistocene ice volume were largely driven by changes in the Laurentide Ice Sheet[29,30].

Initial dust intensification linked to Northern Hemisphere cooling in the mid-Pliocene

Previous studies have suggested that both land-ocean connections and atmospheric circulation may have played key roles in both the oNHG[31] and iNHG[7]. Combined with terrestrial vegetation and atmospheric
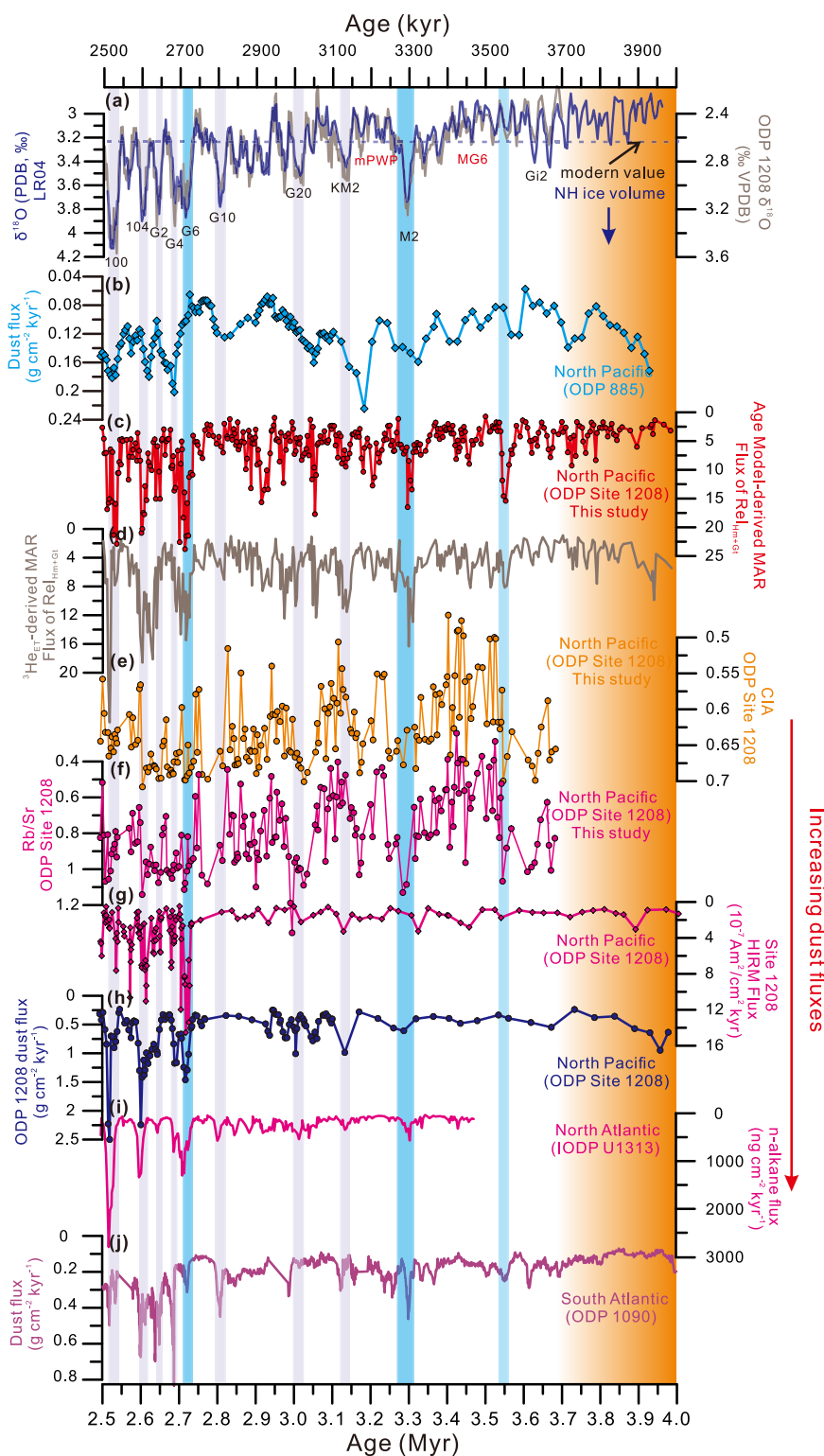
Fig. 2 | Comparison of ODP Site 1208 dust records with data from other sites. **a** Benthic δ^{18}O record at ODP Site 1208 along with the LR04 curve[28]; (**b**) Dust flux at Site 885[13]; (**c**) Rel$_{Hm+Gt}$ flux calculated based on the age model at ODP Site 1208 (this study); (**d**) Rel$_{Hm+Gt}$ flux calculated from [3]He-derived MARs[13] at ODP Site 1208 (this study); (**e**) Chemical index of alteration (CIA) and (**f**) Rb/Sr at ODP Site 1208 (this study); (**g**) Hard Isothermal Remanent Magnetization (HIRM) flux from ODP Site 1208[14]; (**h**) Th and [3]He$_{ET}$-derived dust fluxes from ODP Site 1208[13]; (**i**) Site U1313 dust flux[15]; (**j**) Ti-based dust fluxes from ODP Site 1090[16]. The dark blue bars indicate the onset of NHG (~3.6 Ma), MIS M2 and the iNHG (MIS G6). Light blue bars indicate subsequent glacial intervals. Rel$_{Hm+Gt}$, Relative concentration of haematite and goethite. MIS, Marine Isotope Stage; NHG, Northern Hemisphere Glaciation.
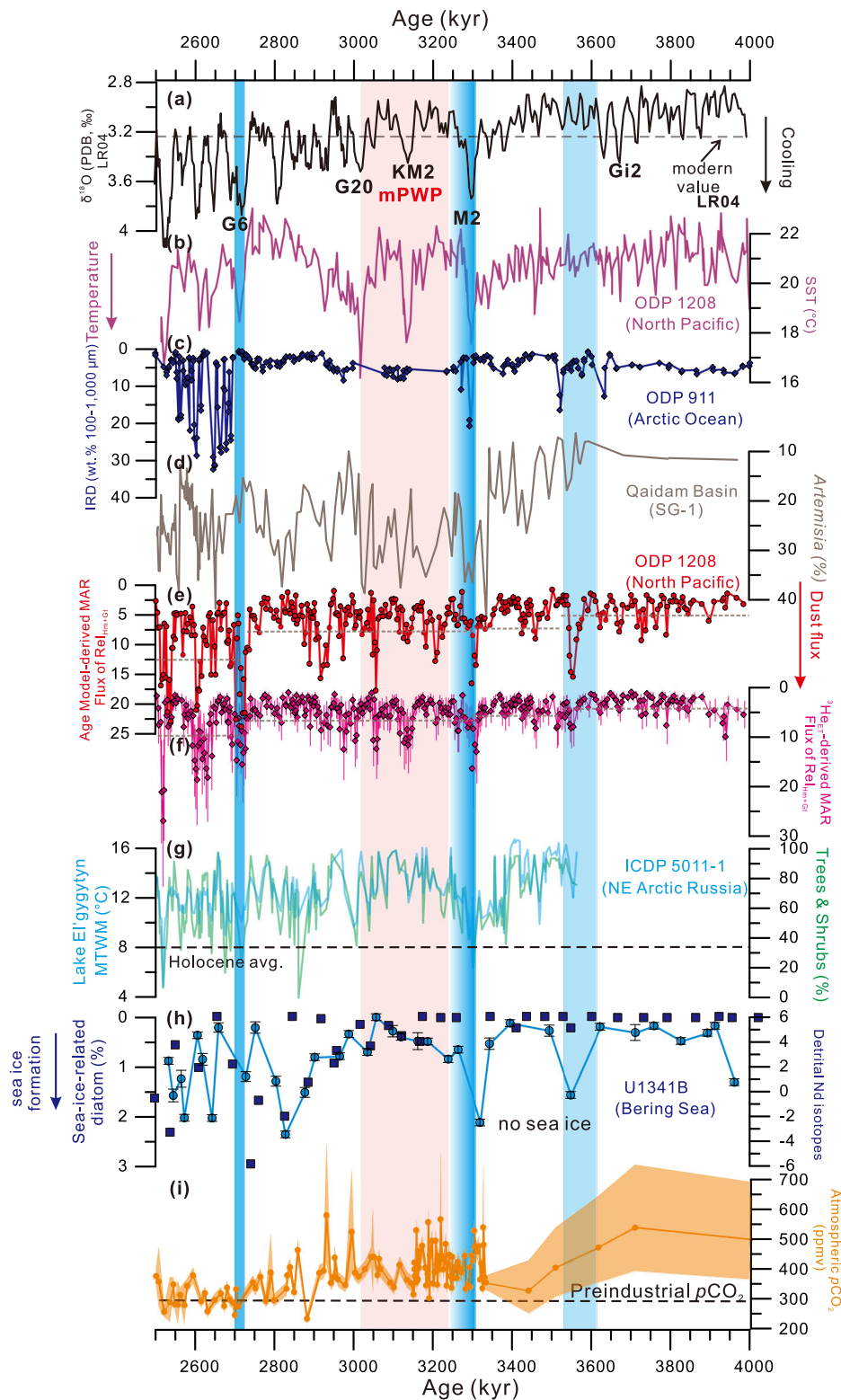
Fig. 3 | Dust flux at ODP Site 1208 compared with global and regional records during the Late Pliocene. a LR04 benthic oxygen isotope stack[28]; (**b**) ODP Site 1208 alkenone-derived SST records[13]; (**c**) Ice-rafted debris (IRD; wt.%, coarse fraction 100–1000 μm) record from the eastern Atlantic-Arctic gateway[23]; (**d**) *Artemisia* pollen percentages from site SG-1 in the Qaidam Basin[39]; (**e**) Flux of Rel$_{Hm+Gt}$ for ODP Site 1208 (this study); (**f**) Flux of Rel$_{Hm+Gt}$ calculated from ³He-derived MAR[13] for ODP Site 1208 (this study). Error bars represent propagated analytical and statistical uncertainties for ³He$_{ET}$-derived MARs (1σ); The heavy dashed grey lines in

(**e**–**f**) indicate average values for the three time windows discussed in the main text; (**g**) Lake surface temperature and tree/shrub percentage records from Lake El'gygytgyn[41]; (**h**) Sea ice-related diatoms (squares)[45] and detrital Nd isotopes (circles) from Bering Sea Hole U1341B[33]; (**i**) Atmospheric pCO_2 based on planktonic foraminifera δ¹¹B[72]. The dark blue bars indicate the onset of NHG (~3.6 Ma), MIS M2 and the iNHG (MIS G6). Light pink bars indicate mid-Piacenizian warm period (mPWP). Rel$_{Hm+Gt}$, Relative concentration of haematite and goethite. MIS, Marine Isotope Stage; NHG, Northern Hemisphere Glaciation.
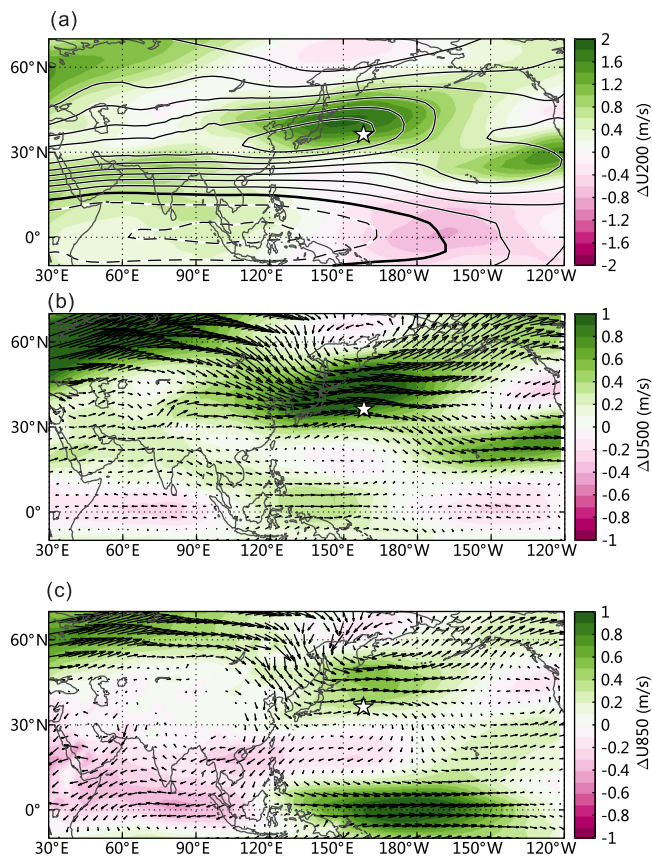
Fig. 4 | Effects of Bering Strait opening on large-scale atmospheric circulation during Pliocene. a 200 hPa zonal wind speed anomalies (shadings; positive values indicate stronger westerlies) and climatological 200 hPa zonal wind pattern (solid contours: westerly winds; dashed contours: easterly winds; thick solid contours: zero contour line; the contour interval is 5 m/s). **b** Anomalies in wind pattern (vectors) and speed (shadings) at 500 hPa. **c** As in (**b**) but for 850 hPa winds. The white star indicates the location of ODP Site 1208. Anomalies indicate the differences between open and closed BS conditions (i.e., open BS climate minus closed BS climate).

circulation records from the Northern Hemisphere, our dust record from ODP Site 1208 (Fig. 3e and f) reveals two temporally distinct modes of mechanisms responsible for cooling over the Pliocene: Mode 1 (3.6–3.3 Ma) and Mode 2 (3.3–2.5 Ma) (Supplementary Fig. 2). Mode 1 (3.6–3.3 Ma) is characterized by variations in Earth-surface dynamics in Central Asia that are connected to shifts in other components of the climate system farther afield (Supplementary Fig. 2a). Initially, during the oNHG from ca. 3.6–3.5 Myr ago, there was a reduction of the North Atlantic Current (NAC) and thus AMOC as indicated by surface-water cooling (ca. 3.5 °C) and freshening in the North Atlantic Ocean (Supplementary Fig. 3b, c). The AMOC reduction might have been driven by increased inflow of low-salinity Pacific waters through the Bering Strait into the Arctic and North Atlantic Oceans[32]. This is evidenced by the growth of large alpine glaciers from ca. 3.6 Myr ago, which produced increasing influxes of Alaska Range detritus and glacial meltwater to the Bering Sea[33].

A mechanistic link between the opening of the Bering Strait and NHG has been suggested for the late Pliocene to explain a reduction in AMOC[34,35]. However, the Bering Strait likely opened much earlier. Recent geological and biogeographic evidence indicates that the Bering Strait was already persistently open around 5.5 Myr ago[36]. If the opening of this gateway is connected to the strength of AMOC, then together these findings imply that Bering Strait was open for a protracted period during which the sill was deep enough to allow the

arrival of Pacific mollusc faunas into the Atlantic Ocean as early as 5.5 Ma, but not enough to substantially alter Arctic and North Atlantic Ocean surface water properties.

Here, we hypothesize that the deepening of Bering Strait below the required threshold was the westward tectonic extrusion of the Bering Block in response to a reactivation of the subduction of the Pacific plate below the Alaska-Aleutian arc[36]. The likely appearance of mountain glaciers in Alaska by the time of MIS M2 at ca. 3.3 Myr ago[3,4] is consistent with enhanced uplift of the central Alaska Range in response to accelerated Pacific plate subduction, extrusion of the Bering block, and deepening of the strait by the mid-Pliocene[36,37]. Coupled with broadly simultaneous tectonic uplift and enhancement of IRD deposition in the Fram Strait area[23] (Fig. 3c), this suggests that tectonic events, surface uplift and the subsequent inception of mountain glaciers preconditioned the peri-Arctic region to stimulate AMOC weakening already by ca. 3.6 Myr ago.

Comparing modelling results based on an open and closed Bering Strait under Pliocene boundary conditions[34], we further demonstrate that a weaker AMOC, driven by the persistent inflow of relatively fresh Pacific waters through an open Bering Strait, could reduce northward heat transport in the North Atlantic and lead to a steepening of the meridional temperature gradient in the Northern Hemisphere (Supplementary Fig. 4). Such a steepened gradient in an open Bering scenario would strengthen the mid-latitude jet stream and westerly winds in the mid to lower troposphere (200–850 hPa) (Fig. 4), facilitating the transport of Asian dust into the North Pacific. Similar effects on the meridional temperature gradient in the North Pacific Ocean and the westerlies have been modelled to be related to narrowing of the Indonesian seaway[38]. These proposed connections provide a mechanism linking enhanced transport of dust from Asia to the North Pacific Ocean with the oNHG. Furthermore, vegetation and precipitation records from Central Asian dust sources suggest a change towards conditions that are more conducive for chemical weathering during the mid-Pliocene[7,39], leading to enhanced erosion and sediment production. Changes in vegetation and precipitation are consistent with our chemical weathering indicators and elevated dust fluxes in the western and central North Pacific Ocean[8,10] (Fig. 1), which together can be interpreted to reflect increased dust emissions from Central Asia around 3.55 Myr ago. Overall, we propose that enhanced dust input for Mode 1 was driven by increased dust production at the source region and intensified mid-latitude atmospheric circulation, both of which ultimately stem from the export of low-salinity waters from the Bering Sea to the Arctic and then North Atlantic Oceans around 3.6 Myr ago.

Enhanced Northern Hemisphere westerlies during major Pliocene glaciations
Our proposed Mode 2 corresponds to changes in the relative influence of the westerlies and the Siberian High that impacted Asian dust emissions, transport, and deposition[40] (Supplementary Fig. 2b). During the middle (ca. 3.4–3.3 Myr ago) and late Pliocene (ca. 2.9 and post 2.7 Myr ago), cool and arid conditions were widespread across central Eurasia as recorded in sediments from Lake Baikal[41], Arctic Siberia[42] (Fig. 3g), and the Tarim Basin[43]. Sea surface temperatures at ODP Site 1208 cooled by 2–4 °C in the western mid-latitude North Pacific during glacial periods of the mid to late Pliocene (i.e., glacial MIS M2 and post-iNHG)[13] (Fig. 3b). This mid-latitude cooling, in conjunction with relatively small changes in tropical SSTs, could reflect an increase in the meridional temperature gradient, resulting in the migration and intensification of Northern Hemisphere westerly winds[12,13].

Modern observations of dust activity indicate that several factors influence dust emissions, including surface wind speed, gustiness, vegetation cover, and soil wetness[44]. To assess the potential of changing dust flux during mid and late Pliocene glaciations, we further
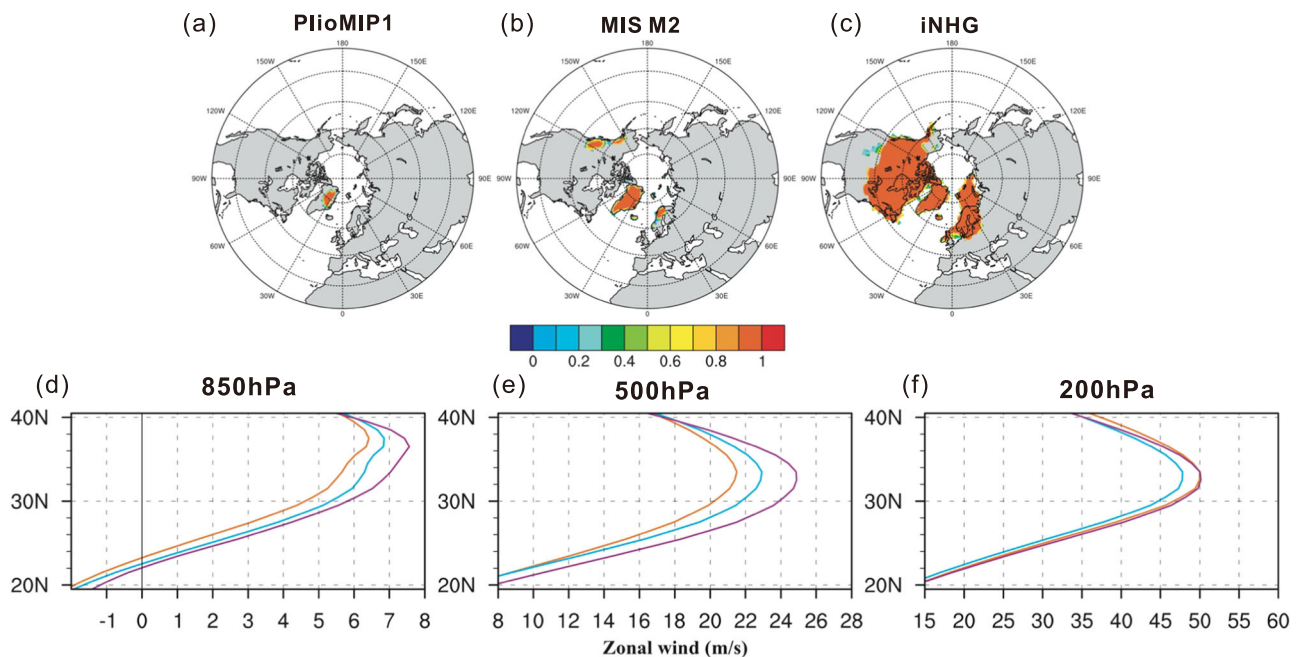
Fig. 5 | Modelled ice sheet and zonal wind changes under three climate conditions. The shaded colour in (**a**–**c**) indicates the land ice fraction. Average zonal winds at different pressure levels (**d**–**f**) are calculated for longitudes between 120°E and 150°E, corresponding to the dominant dust source region for the North Pacific. The orange, blue, and purple curves represent PlioMIP1, MIS M2, and iNHG simulations, respectively. The 850 hPa, 500 hPa and 200 hPa pressure levels generally correspond to altitudes of ~1.5 km, ~5.5 km and, ~12 km, respectively, but can vary due to air conditions and geographic locations. MIS, Marine Isotope Stage; NHG, Northern Hemisphere Glaciation.

analysed modelling results representing the climate of the mPWP, MIS M2 and iNHG (see Methods). In the three scenarios, the extent of NHIS differs substantially between glacial and interglacial periods. During the cold intervals of the mPWP, the Northern Hemisphere continental ice was restricted to Greenland (Fig. 5a). We note, however, that continental ice may have covered the mountainous regions of Alaska and northern Scandinavia during glacial M2[6,7] (Fig. 5b). The growth of Alaskan alpine glaciers during glacial M2 is supported by increasing fluxes of detritus from the Alaska Range at Site U1341 in the Bering Sea (Fig. 3h), possibly due to seasonal glacial meltwater[45]. The major growth of the NHIS occurred during the iNHG (ca. 2.7 Myr ago)[31] and is represented by the LGM NHIS scenario in our model simulations. We note that this is probably an overestimation of Northern Hemisphere ice volume (Fig. 5c), but it may represent a possible scenario for the extent of the Laurentide ice-sheet as reported previously[46]. We chose this extreme scenario to investigate the sensitivity of the atmospheric circulation to changes in ice sheet extent under Pliocene boundary conditions. Compared to the warmer mPWP, the two glacial scenarios considered (glacial M2 and post-iNHG glacials) experienced a decrease in both summer precipitation and evaporation over East, South, and Central Asia. However, the simulations show that the reduction in evaporation caused by cooling exceeded the reduction in precipitation, driving a slightly positive change in the soil moisture budget (precipitation minus evaporation) over inland Asia, which may have helped maintain soil moisture during glacial periods (Supplementary Fig. 5), and further increased weathering and could favour the formation of fine-grained dust to some extent[8].

Aside from just increased dust formation, the characteristics of winds driving dust transport are also different between our simulations. Specifically, our model results suggest that changes in mid-latitude wind circulation play an additional role in enhanced dust flux at our core site. With the build-up of a more extensive NHIS, zonal winds increased at 850 and 500 hPa levels (Fig. 5d–f). The average zonal wind along 120°E–150°E became stronger throughout the year during glacial

M2 and following the iNHG, with wind strength being even stronger during the latter (Fig. 5d, e; Supplementary Fig. 6).

Modern studies show that the strength of the westerlies is related to the meridional temperature gradient[47]. Relatively stronger westerly winds during glacial M2 and the iNHG in the lower and middle atmospheric layers are associated with an increased meridional temperature gradient (Supplementary Fig. 7a, b). However, this is not the case in the upper troposphere. The meridional temperature gradient during glacial M2 is stronger than that during iNHG, but the latter experienced stronger westerly wind speeds (Supplementary Fig. 7c). Notably, modelling of the dust cycle has shown that the main transport of dust occurs below the middle troposphere (3–6 km)[48]. As such, the westerly winds in the upper troposphere do not contribute significantly to the total dust transport in the Northern Hemisphere, in contrast to long-range dust transport in the Southern Hemisphere[49]. Therefore, we suggest that the westerly winds in the lower to middle troposphere promoted dust transport from the interior of Asia to the North Pacific when a larger NHIS formed in the mid-Pliocene (MIS M2) and post-iNHG.

Implications for future climate change
Our North Pacific dust flux record and modelling results aid in better characterizing large-scale Northern Hemisphere Pliocene glaciation events and their associated impacts. In particular, our work (1) provides evidence for long-term Northern Hemisphere ocean-atmosphere-land interactions associated with the oNHG and iNHG, (2) points to enhanced dust production during the intense Pliocene glacial interval M2 that is likely linked to shifts in atmospheric circulation, and (3) supports existing evidence that the iNHG was associated with increased meridional temperature gradients and a strengthening of the westerlies[13–15].

Although the controls on Northern Hemisphere westerlies are determined by stepwise glacial expansion, the response of Earth's surface dynamics to Plio-Pleistocene climatic change in continental

landscape likely generated terrestrial feedbacks affecting atmospheric circulation. We propose that this redistribution of global water vapour linked to North Atlantic ocean-atmosphere feedback was coupled with the reorganization of vegetation patterns in Central Asia[7,39] (Fig. 3d). There is also evidence that East and Central Asia experienced multiple steps of C_4 vegetation expansion through the Pliocene, depending on local monsoon rainfall[50]. Collectively, this significant regional vegetation expansion was common at least in Northwest Australia[51], and the Indian subcontinent[52,53] (Supplementary Fig. 8). At the oNHG, the major dust pulse (Fig. 3e and Supplementary Fig. 8d) was intrinsically linked to regional vegetation change (Supplementary Fig. 8), thus showing the coupling between ice-sheet growth (Supplementary Fig. 8a), land-surface and ocean-atmosphere systems. Moreover, the increased inland weathering and C_4 expansion would have induced additional feedbacks related to the carbon cycle[54] (Supplementary Fig. 3e).

With respect to anthropogenic warming, the high-latitude Northern Hemisphere shows a larger magnitude of warming than at lower latitudes because of the polar amplification, while at the same time a proposed slowdown of the AMOC is expected to result from North Atlantic cooling and freshening[55]. Based on our Pliocene data and modelling, these changes will likely cause counteracting impacts on the mid-latitude westerlies, which has important implications for future climate conditions across the Northern Hemisphere. A comprehensive understanding of these processes regarding large-scale climate system feedbacks, atmospheric circulation, and dust production is necessary to better represent these components of the climate system in climate models to provide improved projections of future climate change.

Methods

Core locations and age models

ODP Site 1208 (36.1°N, 158.2°E, 3,346 m water depth) was drilled on the Shatsky Rise in the western North Pacific[56]. We use a combined ago model and linear interpolation between age tie points to determine our sample ages. The age model[18] is based on a benthic $\delta^{18}O$ record tuned to the LR04 benthic stack[28] for the period of ca. 1.7–3.7 Myr ago and astronomically-tuned paleomagnetic reversal boundaries for the remainder of our record to ca. 4.1 Myr ago[57].

Calculation of dust components from magnetic proxies

Diffuse Reflectance Spectroscopy (DRS) was measured for all samples using a Cary 5000 ultraviolet-visible-infrared spectrometer equipped with $BaSO_4$ as the white standard. DRS data were transformed into the Kubelka-Munk (K-M) remission function using:

$$F(R) = (1 - R)^2 / 2R \qquad (1)$$

where R is reflectance.

The band intensities for haematite and goethite from second derivative curves of F(R) are defined as I_{Hm} and I_{Gt}, which are proportional to the concentration of haematite and goethite[58,59]. Rock magnetic properties were measured in the Centre for Marine Magnetism (CM^2), Southern University of Science and Technology (China).

Our aeolian proxy is defined as Rel_{Hm+Gt}, which is the sum of I_{Hm} and I_{Gt}[22]. To determine the input history of haematite and goethite at ODP Site 1208, we derive the flux of Rel_{Hm+Gt} using two different approaches. The first uses the traditional method based on depth-age tie-points via the equation:

$$\text{Flux of } Rel_{Hm+Gt} = Rel_{Hm+Gt} * DBD * LSR \qquad (2)$$

where DBD represents dry bulk density and LSR stands for linear sedimentation rate. DBD data are calculated by linear interpolation of

shipboard data[56]. The second approach utilizes the constant flux proxy extra-terrestrial ^3He:

$$\text{Flux of } Rel_{Hm+Gt} = Rel_{Hm+Gt} * MAR_{CFP} \qquad (3)$$

where MAR_{CFP} is the vertical sediment mass accumulation rate, independently of lateral sediment advection by bottom currents and age model tie-point interpolation[13].

Geochemical and Pb isotopic analysis

Geochemical analysis of major and trace element concentrations was performed on the siliciclastic fraction of a total of 191 sediment samples from ODP Site 1208. After removal of organic matter, carbonate and Fe-Mn oxides by treating with 10% H_2O_2 at 60 °C for 1 h and 0.5 N HCl at 60 °C for 2 h, respectively, the sediments were rinsed with deionized water three times and dried at 80 °C before grinding into powder. The pre-treated sediments were then digested by a mixture of concentrated HF, HNO_3, and $HClO_4$ in Teflon vessels for elemental analysis. Major and trace element concentrations were determined at the Qingdao Sparta Analysis & Test Co., Ltd., using a Varian 720ES ICP-OES and a Thermo Scientific™ iCAPQ ICP-MS, respectively. Several USGS and Chinese rock and sediment standards (BHVO-2, GBW07315 and GBW07316), as well as procedural blanks, were repeatedly digested and analysed in parallel with the samples to monitor the quality of ICP-MS and ICP-AES measurements. The results are generally within the range of ± 6% of the certified values. The analytical precision is generally better than 3% for major elements and 5% for the trace elements.

We assess the chemical weathering intensity of the source sediments via the chemical index of alteration (CIA). The CIA is based on the relative mobility of Na, K, and Ca in aqueous fluids, compared to immobile Al that tends to be concentrated in the residues of weathered rocks[60]. CIA is calculated as follows: $CIA = [Al_2O_3/(Al_2O_3 + CaO^* + Na_2O + K_2O)] \times 100$ (ref. [61]). CaO^* represents the calcium content from the silicate fraction of the terrigenous sediments, which had been corrected for calcium phosphate and calcium carbonate contents in this study.

Pb isotopic compositions of the silicate fractions from ODP Site 1208 samples were measured following digestion with a mixture of distilled HF and HNO_3 and purification using conventional ion-exchange chromatography. Isotopic analysis was performed using a Nu Instruments multi-collector ICP-MS housed at the State Key Laboratory of Isotope Geochemistry, Guangzhou Institute of Geochemistry, Chinese Academy of Sciences. Internal analytical uncertainty was estimated based on repeated measurements of the Pb reference material NIST 981, using Tl-doping for mass bias correction[62], yielding an internal reproducibility better than 200 ppm/amu for Pb isotopic ratios. Repeated analyses of the USGS rock reference material W-2a gave a reproducibility of $^{206}Pb/^{204}Pb = 16.946 \pm 0.001$, $^{207}Pb/^{204}Pb = 15.506 \pm 0.001$, $^{208}Pb/^{204}Pb = 36.745 \pm 0.001$ (2sd, $n = 30$).

Climate model and simulations

Mode 1 simulations. To contextualize and improve our understanding of the proxy results ca. 3.6 Myr ago, we use a set of Pliocene climate simulations reported in Otto-Bliesner et al. [34]. This set of simulations was conducted with the Community Climate System Model version 4 (CCSM4)[63], which has fully coupled atmosphere (Community Atmosphere Model, version 4, CAM4), land (Community Land Model, version 4, CLM4), ocean (Parallel Ocean Program, version 2, POP2), and sea ice (Community Sea Ice Model, version 4, CICE4) components. The atmosphere and land components were run at a 0.9° × 1.25° horizontal resolution, and the ocean and sea ice components were run with a common grid of 320 × 384 points. The baseline simulation follows the PlioMIP1 forcing protocol, with atmospheric CO_2 of 405 ppmv (parts per million by volume) and the Pliocene Research, Interpretation, and

Synoptic Mapping, version 3 (PRISM3) boundary conditions. Notably, PRISM3 includes an open Bering Strait (BS) and Canadian Archipelago Straits (CA)[64], both of which have since been changed to closed in the updated PRISM4 Pliocene topography[65,66].

In this study, we use two of the Arctic gateway sensitivity tests reported in Otto-Bliesner et al.[34], including (1) open BS + closed CA, and (2) closed BS + closed CA to test the hypothesis that the opening of the Bering Strait in the late Pliocene strengthens the westerly winds. By comparing the differences between the climate outputs of the two simulations, we can assess the impact of opening/closing of the Bering Strait on global climate. The simulations show that Bering Strait opening as early as 5.5 Ma enables the transport of relatively fresh North Pacific waters to the North Atlantic, which weakens AMOC by freshening North Atlantic surface waters (Supplementary Fig. 4). This weakening of the AMOC, in turn, leads to a reduction in poleward heat transport and thus a steepened meridional temperature gradient (Supplementary Fig. 4). Because westerly wind intensity is strongly controlled by the meridional temperature gradient, a steepened temperature gradient is responsible for intensified the westerly winds as simulated (Fig. 4). Our model results provide a physical mechanism to explain our proxy data reconstructions which show increased dust transport associated with Mode 1 during the mid-Pliocene.

Mode 2 simulations. Climate simulations used to understand Mode 2 of late Pliocene climate change were performed using the Institute Pierre Simon Laplace atmosphere–ocean coupled general circulation model, IPSL-CM5A. The atmosphere component in this AOGCM is the LMDZ5A and the ORCHIDEE land-surface model with a resolution of 3.75° x 1.875° and 39 vertical layers. The ocean model is NEMOv3.2, which includes the ORCA2.3 ocean configuration and uses a tri-polar global grid. More details about the IPSL-CM5A model can be found in Dufresne et al. [67]. In this study, three climate simulations were performed, namely the "PlioMIP1", "MIS M2", and "iNHG" simulations. "PlioMIP1" was performed based on the PRSIM3D boundary conditions[68,69], whereas "MIS M2" was performed by adding different driving factors based on the equilibrated state of "PlioMIP1" in order to represent the onset of MIS M2. Specifically, changes in the Central American seaway, lowering of pCO_2 from 400 ppmv to 220 ppmv, different orbital parameters ca. 3.313 Myr ago, altered vegetation (replacing boreal biomes north of 50°N with tundra biomes based on the PRISM3D vegetation map[70]), and ice-sheet growth were taken into account in this simulation (see Tan et al.[3]. for more details). The "iNHG" simulation was performed using the "PlioMIP 1" palaeogeography, but with a Last Glacial Maximum (LGM) ice-sheet configuration and orbital parameters corresponding to 2.601 Myr ago (for more details, see Tan et al.[4]).

Data availability
Source data are provided with this paper. The data generated in this study have been deposited in the https://doi.org/10.5281/zenodo.10633222.

Code availability
The information for the applied climate model IPSL-CM5A can be found in the IPSL Climate Modelling Centre Wiki page (http://forge.ipsl.jussieu.fr/igcmg) and in Dufresne et al.[67]. Since this version has been updated to a new version, the code of this model is not publicly available, and might be available on quest to the IPSL group. The information for the Community Climate System Model (CCSM4) can be found in (https://www.cesm.ucar.edu/models/ccsm). CCSM4 is now a subset of Community Earth System Model (CESM 1.0). The CCSM4 code base is frozen, and all future model updates will come from the CESM1.0 code base. Figures were plotted with the NCAR Command Language (version NCL 6.4.0). Information on NCL is available at https://www.ncl.ucar.edu/.

References
1. Burke, K. D. et al. Pliocene and Eocene provide best analogs for near-future climates. *Proc. Natl Acad. Sci. USA* **115**, 13288–13293 (2018).
2. McClymont, E. L. et al. Climate evolution through the onset and intensification of Northern Hemisphere glaciation. *Rev. Geophys.* **61**, e2022RG000793 (2023).
3. Tan, N. et al. Exploring the MIS M2 glaciation occurring during a warm and high atmospheric CO_2 Pliocene background climate. *Earth Planet. Sci. Lett.* **472**, 266–276 (2017).
4. Tan, N. et al. Dynamic Greenland ice sheet driven by pCO_2 variations across the Pliocene Pleistocene transition. *Nat. Commun.* **9**, 4755 (2018).
5. Woodard, S. C. et al. Antarctic role in Northern Hemisphere glaciation. *Science* **346**, 847–851 (2014).
6. Haug, G. H. & Tiedemann, R. Effect of the formation of the Isthmus of Panama on Atlantic ocean thermohaline circulation. *Nature* **393**, 673–676 (1998).
7. Prud'homme, C. et al. Central Asian modulation of Northern Hemisphere moisture transfer over the late Cenozoic. *Commun. Earth Environ.* **2**, 106 (2021).
8. Zhang, Q. et al. Mechanism for enhanced eolian dust flux recorded in North Pacific Ocean sediments since 4.0 Ma: Aridity or humidity at dust source areas in the Asian interior? *Geology* **48**, 77–81 (2020).
9. Lambert, F. et al. Dust-climate couplings over the past 800,000 years from the EPICA Dome C ice core. *Nature* **452**, 616–619 (2008).
10. Lambert, F. et al. Centennial mineral dust variability in high-resolution ice core data from Dome C, Antarctica. *Climate* **8**, 609–623 (2012).
11. Ruch, U. et al. Ice core evidence for a very tight link between North Atlantic and East Asian glacial climate. *Geophys. Res. Lett.* **34**, L03706 (2007).
12. Zhong, Y. et al. Humidification of Central Asia and equatorward shifts of westerly winds since the late Pliocene. *Commun. Earth Environ.* **3**, 274 (2022).
13. Abell, J. T., Winckler, G., Anderson, R. F. & Herbert, T. D. Poleward and weakened westerlies during Pliocene warmth. *Nature* **589**, 70–75 (2021).
14. Bridges, J. D., Tarduno, J. A., Cottrell, R. D. & Herbert, T. D. Rapid strengthening of westerlies accompanied intensification of Northern Hemisphere glaciation. *Nat. Commun.* **14**, 3905 (2023).
15. Naafs, B. D. A. et al. Strengthening of North American dust sources during the late Pliocene (2.7 Ma). *Earth Planet. Sci. Lett.* **317–318**, 8–19 (2012).
16. Martínez Garcia, A. et al. Southern Ocean dust-climate coupling over the past four million years. *Nature* **476**, 312–315 (2011).
17. Abell, J. T. et al. Evaluating the drivers of quaternary dust fluxes to the Western North Pacific: East Asian dustiness and Northern Hemisphere gustiness. *Paleoceanogr. Paleoclimatol.* **38**, e2022PA004571 (2023).
18. Venti, N. L. & Billups, K. Stable-isotope stratigraphy of the Pliocene-Pleistocene climate transition in the northwestern subtropical Pacific. *Palaeogeogr. Palaeoclimatol. Palaeoecol.* **326**, 54–65 (2012).
19. Zhang, W., Chen, J., Ji, J. & Li, G. Evolving flux of Asian dust in the North Pacific Ocean since the late Oligocene. *Aeolian Res.* **23**, 11–20 (2016).
20. Weber, E. T. et al. Quantitative resolution of eolian continental crustal material and volcanic detritus in North Pacific surface sediment. *Paleoceanography* **11**, 115–127 (1996).
21. Liu, Q. et al. Characterizing magnetic mineral assemblages of surface sediments from major Asian dust sources and implications for the Chinese loess magnetism. *Earth Planets Space* **67**, 61 (2015).

22. Zhong, Y. et al. Orbital-controlled mid-latitude North Pacific dust flux during the late Quaternary. *Geophys. Res. Lett.* **51**, e2023GL106631 (2024).

23. Knies, J. et al. Effect of early Pliocene uplift on late Pliocene cooling in the Arctic–Atlantic gateway. *Earth Planet. Sci. Lett.* **387**, 132–144 (2014).

24. De Schepper, S., Gibbard, P. L., Salzmann, U. & Ehlers, J. A global synthesis of the marine and terrestrial evidence for glaciation during the Pliocene Epoch. *Earth Sci. Rev.* **135**, 83–102 (2014).

25. Knies, J. et al. The emergence of modern sea ice cover in the Arctic Ocean. *Nat. Commun.* **5**, 5608 (2014).

26. Dolan, A. M. Modelling the enigmatic late Pliocene Glacial event—marine isotope stage M2. *Glob. Planet. Change* **128**, 47–60 (2015).

27. Haywood, A. M. et al. The Pliocene model intercomparison project (PlioMIP) phase 2: scientific objectives and experimental design. *Climate* **12**, 663–675 (2016).

28. Lisiecki, L. E. & Raymo, M. E. A Pliocene-Pleistocene stack of 57 globally distributed benthic δ18O records. *Paleoceanography* **20**, PA1003 (2005).

29. Hughes, P. D. & Gibbard, P. L. Global glacier dynamics during 100 ka Pleistocene glacial cycles. *Quat. Res.* **90**, 222–243 (2018).

30. Hughes, P. D. et al. The "missing glaciations" of the Middle Pleistocene. *Quat. Res.* **96**, 161–183 (2020).

31. Kleiven, H. F., Jansen, E., Fronval, T. & Smith, T. M. Intensification of Northern Hemisphere glaciations in the circum Atlantic region (3.5-2.4 Ma) - ice-rafted detritus evidence. *Palaeogeogr. Palaeoclimatol. Palaeoecol.* **184**, 213–223 (2002).

32. Karas, C. et al. Did North Atlantic cooling and freshening from 3.65–3.5 Ma precondition Northern Hemisphere ice sheet growth? *Glob. Planet. Change* **185**, 103085 (2020).

33. Horikawa, K. et al. Pliocene cooling enhanced by flow of low-salinity Bering Sea water to the Arctic Ocean. *Nat. Commun.* **6**, 7587 (2015).

34. Otto-Bliesner, B. L. et al. Amplified North Atlantic warming in the late Pliocene by changes in Arctic gateways. *Geophys. Res. Lett.* **44**, 957–964 (2017).

35. Hu, A. et al. Effects of the Bering Strait closure on AMOC and global climate under different background climates. *Prog. Oceanogr.* **132**, 174–196 (2015).

36. Hall, J. R., Allison, M. S., Papadopoulos, M. T., Barfod, D. N. & Jones, S. M. Timing and consequences of Bering Strait opening: new insights from 40Ar/39Ar dating of the barmur group (Tjörnes Beds), Northern Iceland. *Paleoceanogr. Paloclimatol.* **38**, e2022PA004539 (2023).

37. Elliott, J. & Freymueller, J. T. A bock model of present-day Kinematics of Alaska and Western Canada. *J. Geophys. Res. Solid Earth* **125**, e2019JB018378 (2020).

38. Tan, N. et al. Recognizing the role of tropical seaways in modulating the Pacific circulation. *Geophys. Res. Lett.* **49**, e2022GL099674 (2022).

39. Koutsodendris et al. Late Pliocene vegetation turnover on the NE Tibetan Plateau (Central Asia) triggered by early Northern Hemisphere glaciation. *Glob. Planet. Change* **180**, 117–125 (2019).

40. Luetscher, M. et al. North Atlantic storm track changes during the Last Glacial maximum recorded by Alpine speleothems. *Nat. Commun.* **6**, 6344 (2015).

41. Williams, D. F. et al. Lake Baikal record of continental climate response to orbital insolation during the past 5 million years. *Science* **278**, 1114–1117 (1997).

42. Brigham-Grette, J. et al. Pliocene warmth, polar amplification, and stepped pleistocene cooling recorded in NE Arctic Russia. *Science* **340**, 1421–1427 (2013).

43. Wang, X. et al. A high-resolution multi-proxy record of late Cenozoic environment change from central Taklimakan Desert, China. *Climate* **9**, 2731–2739 (2013).

44. Rodriguez-Caballero, E. et al. Global cycling and climate effects of aeolian dust controlled by biological soil crusts. *Nat. Geosci.* **15**, 458–463 (2022).

45. Onodera, J., Takahashi, K. & Nagatomo, R. Diatoms, silicoflagellates, and ebridians at site U1341 on the western slope of Bowers Ridge, IODP expedition 323. *Deep Sea Res. Part II Topical Stud. Oceanogr.* **125–126**, 8–17 (2016).

46. Balco, G. & Rovey, C. W. II. Absolute chronology for major Pleistocene advances of the Laurentide Ice sheet. *Geology* **38**, 795–798 (2010).

47. Dong, B., Sutton, R. T., Shaffrey, L. & Harvey, B. Recent decadal weakening of the summer Eurasian westerly jet attributable to anthropogenic aerosol emissions. *Nat. Commun.* **13**, 1148 (2022).

48. Albani, S. et al. Improved dust representation in the community atmosphere model. *J. Adv. Model. Earth Syst.* **6**, 541–570 (2014).

49. Struve, T. et al. Systematic changes in circumpolar dust transport to the Subantarctic Pacific Ocean over the last two glacial cycles. *Proc. Natl Acad. Sci. USA* **119**, e2206085119 (2022).

50. Zhou, B. et al. Late Pliocene–Pleistocene expansion of C4 vegetation in semiarid East Asia linked to increased burning. *Geology* **42**, 1067–1070 (2014).

51. Andrae, J. W. et al. Initial expansion of C4 vegetation in Australia during the Late Pliocene. *Geophys. Res. Lett.* **45**, 4831–4840 (2018).

52. Dunlea, A. G., Giosan, L. & Huang, Y. Pliocene expansion of C4 vegetation in the Core Monsoon zone on the Indian Peninsula. *Clim. Past Discuss.* **16**, 2533–2546 (2020).

53. Huang, Y., Clemens, S. C., Liu, W., Wang, Y. & Prell, W. L. Large-scale hydrological change drove the late Miocene C4 plant expansion in the himalayan foreland and Arabian Peninsula. *Geology* **35**, 531–534 (2007).

54. Berends, C. J. et al. Modelling ice sheet evolution and atmospheric CO2 during the Late Pliocene. *Clim* **15**, 1603–1619 (2019).

55. Rahmstorf, S. et al. Exceptional twentieth-century slowdown in Atlantic ocean overturning circulation. *Nat. Clim. Change* **5**, 475–480 (2015).

56. Bralower, T. J. et al. Shipboard scientifi party. Site 1208. In *Proc. Ocean Drilling Program, Init. Rep.* 198 (2002).

57. Evans, H. F. *Magnetic Stratigraphy and Environmental Magnetism of Oceanic Sediments*. https://archimer.ifremer.fr/doc/00505/61625/ (2006).

58. Scheinost, A. C., Chavernas, A., Barrón, V. & Torrent, J. Use and limitations of second-derivative diffuse reflectance spectroscopy in the visible to near-infrared range to identify and quantify Fe oxide minerals in soils. *Clays Clay Miner.* **46**, 528–536 (1998).

59. Torrent, J., Liu, Q., Bloemendal, J. & Barron, V. Magnetic enhancement and iron oxides in the upper luochuan loess-paleosol sequence, Chinese loess plateau. *Soil Sci. Soc. Am. J.* **71**, 1570–1578 (2007).

60. Nesbitt, H. W. & Young, G. M. Prediction of some weathering trends of plutonic and volcanic rocks based on thermodynamic and kinetic considerations. *Geochimica. et. Cosmochimica. Acta* **48**, 1523–1534 (1984).

61. Nesbitt, H. W. & Young, G. M. Early Proterozoic climates and plate motions inferred from major element chemistry of lutites. *Nature* **299**, 715–717 (1982).

62. Collerson, K. D., Kamber, B. S. & Schoenberg, R. Applications of accurate, high-precision Pb isotope ratio measurement by multi-collector ICP-MS. *Chem. Geol.* **188**, 65–83 (2002).

63. Gent, P. R. et al. The community climate system model version 4. *J. Clim.* **24**, 4973–4991 (2011).

64. Rosenbloom, N. A., Otto-Bliesner, B. L., Brady, E. C. & Lawrence, P. J. Simulating the mid-pliocene warm period with the CCSM4 model. *Geosci. Model Dev.* **6**, 549–561 (2013).

65. Dowsett, H. J. et al. Assessing confidence in Pliocene sea surface temperatures to evaluate predictive models. *Nat. Clim. Change* **2**, 365–371 (2012).

66. Haywood, A. M., Dowsett, H. J. & Dolan, A. M. Integrating geological archives and climate models for the mid-Pliocene warm period. *Nat. Commun.* **7**, 10646 (2016).

67. Dufresne et al. Climate change projections using the IPSL-CM5 earth system model: from CMIP3 to CMIP 5. *Clim. Dyn.* **40**, 2123–2165 (2013).

68. Contoux, C., Ramstein, G. & Jost, A. Modelling the mid-Pliocene warm period climate with the IPSL coupled model and its atmospheric component LMDZ5A. *Geosci. Model Dev.* **5**, 903–917 (2012).

69. Salzmann, U., Haywood, A. M. & Lunt, D. J. The past is a guide to the future? comparing middle Pliocene vegetation with predicted biome distributions for the twenty-first century. Philosophical transactions of the royal society A: mathematical. *Phys. Eng. Sci.* **367**, 189–204 (2008).

70. Pye, K. Processes of fine particle formation, dust source regions, and climatic Changes. In: *Paleoclimatology and Paleometeorology: Modern and Past Patterns of Global Atmospheric Transport.* (eds. Leinen, M., Sarnthein, M.) 1389–2185 (Springer Netherlands, Dordrecht, 1989).

71. Dowsett, H. et al. The PRISM4 (mid-Piacenzian) paleoenvironmental reconstruction. *Climate* **12**, 1519–1538 (2016).

72. Rae, J. W. B. et al. Atmospheric CO_2 over the past 66 million years from marine archives. *Annu. Rev. Earth Planet. Sci.* **49**, 609–641 (2020).

Acknowledgements

Author contributions

Y.Z., and Q.S.L. designed the project. Y.Z., N. T., J.T.A., S.K.B., H.L.F., T.D.H., A.P., K.H., T.S., M.E.W., J.M.Y., P.D.C., J.C.L., A.B., and T.C. prepared the first draft of the manuscript. S.Y. completed the sample collection. W.C. was responsible for sample preparation. Y.Z., J.T.A., J.Y.Z., and W.Y.X. were responsible for data collection and/or synthesis. N.T., C.J.S., Z.Y.L., and H.Y. assisted with model simulations.

Competing interests

The authors declare no competing interests.

Additional information

Supplementary information The online version contains supplementary material available at https://doi.org/10.1038/s41467-024-51127-w.

Correspondence and requests for materials should be addressed to Yi Zhong, Ning Tan or Qingsong Liu.

Peer review information *Nature Communications* thanks Julie Brigham-Grette and the other, anonymous, reviewer for their contribution to the peer review of this work. A peer review file is available.

Reprints and permissions information is available at http://www.nature.com/reprints

Publisher's note Springer Nature remains neutral with regard to jurisdictional claims in published maps and institutional affiliations.

¹Centre for Marine Magnetism (CM2), Department of Ocean Science and Engineering, Southern University of Science and Technology, Shenzhen 518055, PR China. ²Key Laboratory of Cenozoic Geology and Environment, Institute of Geology and Geophysics, Chinese Academy of Sciences, Beijing 100029, China. ³Department of Earth and Environmental Sciences, Lehigh University, Bethlehem, PA 18015, USA. ⁴Department of Geosciences, University of Arizona, Tucson, AZ 85721, USA. ⁵Department of Earth and Planetary Sciences, University of California Davis, Davis, CA 95616, USA. ⁶Institute of Geological Sciences, Freie Universität Berlin, Berlin 12249, Germany. ⁷School of Geography, Queen Mary University of London, London, UK. ⁸Department of Earth, Environmental and Planetary Sciences, Brown University, Providence, RI 02912, USA. ⁹Department of Environmental Engineering and Earth Sciences, Clemson University, Clemson, SC 29634, USA. ¹⁰Faculty of Science, Academic Assembly, University of Toyama, Toyama, Japan. ¹¹Laoshan Laboratory, Qingdao, China. ¹²Research School of Earth Sciences, Australian National University, Canberra, Australia. ¹³Marine Isotope Geochemistry, Institute for Chemistry and Biology of the Marine Environment (ICBM), University of Oldenburg, 26129 Oldenburg, Germany. ¹⁴Institute for Geosciences, Department of Geochemistry and Petrology, University of Bonn, Bonn, Germany. ¹⁵Department of Earth Sciences, University College London, London WC1E 6BS, UK. ¹⁶Departamento de Ciencias, Universidad Pública de Navarra, 31006 Pamplona, Spain. ¹⁷IGME, CSIC, Zaragoza Headquarters, Campus Aula Dei, 50059 Zaragoza, Spain. ¹⁸Department of Physical Geography and Ecosystem Science, Lund University, Lund, Sweden. ¹⁹Southern Marine Science and Engineering Guangdong Laboratory, Zhuhai, China. ²⁰Institute of Earth Sciences, Heidelberg University, Heidelberg 69120, Germany. ²¹State Key Laboratory for Mineral Deposit Research, School of Earth Sciences and Engineering, Nanjing University, Nanjing 210023, China. ²²Shanghai Sheshan National Geophysical Observatory, Shanghai, China. ✉e-mail: zhongy@sustech.edu.cn; ning.tan@mail.iggcas.ac.cn; qsliu@sustech.edu.cn